Naval Research Laboratory

Washington, DC 20375-5320

NRL/MR/6750--11-9331

Plasma Diagnostics with a High Aspect Ratio Cylindrical Probe Used as an Impedance Probe

D.N. WALKER

Sotera Defense Solutions, Inc.
Crofton, Maryland

R.F. FERNSLER
D.D. BLACKWELL
W.E. AMATUCCI

Charged Particle Physics Branch
Plasma Physics Division

May 27, 2011

REPORT DOCUMENTATION PAGE

Form Approved
OMB No. 0704-0188

1. REPORT DATE *(DD-MM-YYYY)*	**2. REPORT TYPE**	**3. DATES COVERED** *(From - To)*
27-05-2011	Memorandum Report	

4. TITLE AND SUBTITLE

Plasma Diagnostics with a High Aspect Ratio Cylindrical Probe Used as an Impedance Probe

5a. CONTRACT NUMBER

5b. GRANT NUMBER

5c. PROGRAM ELEMENT NUMBER

6. AUTHOR(S)

D.N. Walker,* R.F. Fernsler, D.D. Blackwell, and W.E. Amatucci

5d. PROJECT NUMBER
67-9872-01

5e. TASK NUMBER

5f. WORK UNIT NUMBER

7. PERFORMING ORGANIZATION NAME(S) AND ADDRESS(ES)

Naval Research Laboratory
4555 Overlook Avenue, SW
Washington, DC 20375-5320

8. PERFORMING ORGANIZATION REPORT NUMBER

NRL/MR/6750--11-9331

9. SPONSORING / MONITORING AGENCY NAME(S) AND ADDRESS(ES)

Office of Naval Research
875 North Randolph Street, Suite 1425
Arlington, VA 22203-1995

10. SPONSOR / MONITOR'S ACRONYM(S)

ONR

11. SPONSOR / MONITOR'S REPORT NUMBER(S)

12. DISTRIBUTION / AVAILABILITY STATEMENT

Approved for public release; distribution is unlimited.

13. SUPPLEMENTARY NOTES

*Sotera Defense Solutions, Inc., Crofton, MD

14. ABSTRACT

Using a network analyzer to supply a driving rf signal to varying sizes of spherical probes in plasma, we have performed plasma diagnostics using theory based on an assumption of a thin sheath and a collisionless plasma. The rf signal applied to the probe by the network analyzer is small in magnitude compared to probe bias voltages and the instrument returns both real and imaginary parts of the complex plasma impedance as a function of frequency for given bias voltages. This information can be used to determine plasma potential, electron density and temperature, in addition to the electron distribution function. Further, we have shown that sheath resistance and sheath density profiles are also a product of the method. The theoretical basis of the work indicates that in the thin sheath limit the results should be independent of probe geometry. To test this we have used a 100-l (length – radius) aspect ratio cylinder which we also sweep as a Langmuir probe. We compare the impedance-based plasma measurements to those of the cylinder when swept as a Langmuir probe using conventional algorithms to reduce the I-V characteristic.

15. SUBJECT TERMS

Plasma sheath
Collisionless plasma
Plasma impedance
Plasma potential

16. SECURITY CLASSIFICATION OF:			**17. LIMITATION OF ABSTRACT**	**18. NUMBER OF PAGES**	**19a. NAME OF RESPONSIBLE PERSON**
a. REPORT	**b. ABSTRACT**	**c. THIS PAGE**			Richard F. Fernsler
Unclassified	Unclassified	Unclassified	UL	16	**19b. TELEPHONE NUMBER** *(include area code)* (202) 767-6786

Standard Form 298 (Rev. 8-98)
Prescribed by ANSI Std. Z39.18

TABLE OF CONTENTS

I. Introduction

We have previously demonstrated the usefulness of network analyzers for plasma diagnostics using spheres of various sizes.[1-4] In the most recent work[3,4] we demonstrated a method of determining plasma potential and the electron energy distribution from which electron temperature can be estimated. In the present note we apply the same algorithms to a cylindrical probe of length L = 15 cm and radius r = .16 cm. This work will not repeat the theoretical framework but will present those equations used in the analysis with only a very brief description. Interested readers are referred to the earlier works which form the theoretical basis of the technique used.[1-4,8]

II. A Brief Overview of the Algorithm

Electron density is determined as with conventional impedance probes by applying a small rf signal and determining plasma resonance in the real part of the impedance $Re(Z_{ac})$ and also by the change in the imaginary part $Im(Z_{ac})$ from capacitive to inductive (*i.e.*, a zero crossing indicating vanishing reactance).[1] As an approximation, the bulk plasma behaves as inductance whereas the sheath region near the probe can be characterized as an ac resistance, R_{ac}, in parallel with an ac capacitance, C_{ac}. Since the network analyzer provides both $Im(Z_{ac})$ and $Re(Z_{ac})$, there are two identifiers of plasma frequency.

The determination of the electron distribution function, $f(\varepsilon)$[3,4], electron temperature[2], T_e , and plasma potential[3], φ_p, requires that we operate in the frequency range $\omega_{pi} < \omega < \omega_{pe}(r_0)$, where ω_{pi} is the ion plasma frequency, ω is the applied network analyzer frequency, and $\omega_{pe}(r_0)$ is the electron plasma frequency at the surface of the probe with radius r_0. Because of the frequency range, the ac ion current is small and the ac resistance is given by[2],

$$R_{ac} = \left(\frac{dI_e}{dV_p}\right)^{-1} \tag{1}$$

where I_e is the dc electron current at bias voltage V_p *i.e.*, the total ac current is now largely electron current. The Druyvesteyn[7] equation may now be expressed in terms of a first order derivative or,

$$f(\varepsilon) = \frac{4}{e^3 A_p}\sqrt{\frac{m_e \varepsilon}{2}}\left(\frac{dR_{ac}^{-1}}{dV_p}\right)_{eV_p=-\varepsilon} \tag{2}$$

and thus noise is reduced in the calculation of the distribution function, where A_p is the probe area, m_e is electron mass, and ε is the energy. In addition, earlier work[2] demonstrates the relationship between the real part of the analyzer output and R_{ac},

Manuscript approved April 6, 2011.

$$\mathrm{Re}(Z_{ac}) = \frac{R_{ac}}{1+(\omega R_{ac} C_{ac})^2}. \qquad (3)$$

Therefore, in the frequency range given, and provided $\omega R_{ac} C_{ac} << 1$, we have $Re(Z_{ac}) \approx R_{ac}$ and $Re(Z_{ac})$ from the network analyzer output can be directly used in place of R_{ac} in Eqn (2). This simplifies finding $f(\varepsilon)$ by avoiding a calculation for R_{ac} when reducing the data. For comparison purposes, we use both methods of finding $f(\varepsilon)$; one which relies on finding R_{ac} and the other which uses $Re(Z_{ac})$ directly. Once $f(\varepsilon)$ is known we can estimate T_e assuming a Maxwellian distribution and by further integration find another estimate of the electron density for consistency comparison.

Since the basis for determining plasma potential is that d^2I_e/dV_p^2 vanishes at $V_p = \varphi_p$,

$$\left.\frac{dR_{ac}}{dV_p}\right|_{V_p=\phi_p} = -R_{ac}^2 \left.\left(\frac{d^2 I_e}{dV_p^2}\right)\right|_{V_p=\phi_p} = 0 \qquad (4)$$

and finally,

$$\left.\frac{d\,\mathrm{Re}(Z_{ac})}{dV_p}\right|_{V_p=\phi_p} \simeq 0 \qquad (5)$$

Plots of the network analyzer output of $Re(Z_{ac})$ versus applied bias for frequencies in the range specified will then show a minimum at $V_p = \varphi_p$. Due to the dependence of $f(\varepsilon)$ on dR_{ac}^{-1}/dV_p seen in Eq (2) we are able to construct $f(\varepsilon)$ (Figure 3) in the vicinity of φ_p for small negative bias voltages and from this derive n_e (Figure 4) and T_e (Figure 5) as will be covered below.

III. Outline of Experimental Procedure

We refer the reader interested in the experimental details to the earlier works and only provide an outline of that same description here.

The experiments were conducted using as a probe a stainless steel cylinder with length, L = 15 cm and radius, r = 0.16 cm which is connected to an HP8735D Network Analyzer through 50 Ω coaxial cable which provides the driving signal. This arrangement including the chamber, analyzer and the coupling circuitry is shown schematically in Reference 2. The cylinder is mounted on a 1/4 inch diameter ceramic and steel support which is connected to 1/4 inch diameter semi-rigid copper 50 Ohm coaxial cable.

The determination of plasma impedance depends upon the network analyzer measurement of the complex reflection coefficient, $\Gamma(\omega)$. The analyzer returns as separate outputs $Re\ Z_{ac}(\omega)$ and $Im\ Z_{ac}(\omega)$ where,

$$Z_{ac}(\omega) = Z_0[\frac{1+\Gamma(\omega)}{1-\Gamma(\omega)}] \quad (6)$$

and Z_0 (=50 Ω) is the internal impedance of the analyzer. We also note that the ratio of reflected-to-total power is given by,

$$|\Gamma|^2 = \frac{P_r}{P_0} \quad (7)$$

where $P_0 = P_R + P_T$ with P_R and P_T the reflected and transmitted powers, respectively. (The quantity $1 - |\Gamma|^2$ is the normalized transmitted power and this output is also available).

IV. Results and Discussion

We compare two data sets taken under similar plasma conditions on different days with the probe aligned along the magnetic field direction. The magnetic field was ~ 2 gauss and is primarily employed to contain the plasma radially by inhibiting diffusion to the walls.

IV.1 Electron densities from Re(Z_{ac}) and Im(Z_{ac})

Figures 1 and 2 show the impedance probe results for the 2 cases. The *Re(Z_{ac})* shows resonance at the plasma frequency and the *Im(Z_{ac})* shows the zero crossing indicating the transfer of total power into the real part of the impedance at resonance. These densities are compared below to their values using alternate methods.

IV.2 Magnetic field effects in cylindrical Langmuir probe data analysis

With the probe aligned along B, magnetic field effects under certain restrictions can decrease the collected electron current and therefore Langmuir probe determination of density based on electron saturation current collection indicates an artificially lower bulk plasma value than is the actual case. Because of this, electron temperature determinations can also be compromised since most fitting routines use the entire IV characteristic in the fit itself. The effects of magnetic fields on both spheres and cylinders have been studied over the years[5,6], and it is not the intention here to retrace that work although some general comments are appropriate when comparing to impedance probe measurements. The magnitude of the effect depends on the electron gyroradius, r_e, in addition to the size and shape of the probe and its sheath. In a thin sheath limit, and assuming the same applied bias, we expect generally less influence as a function of probe orientation with respect to $\boldsymbol{B}$ as probe radius, r, decreases with respect to r_e. In the present case the sheath radius, r_{sh} is estimated at 0.5 cm (assuming $r_{sh} \sim 5\lambda_D$) while the cylinder radius is 0.16 cm or $r_{sh} > r$. Also, since r_e/r for a 2 gauss confining field is of order 10 for a typical T_e of *1 eV*, we expect less of an effect than would be the case for a

lower ratio. However, it has been shown for cylindrical probes that even when $r_e > r$ magnetic fields can be important and, in addition, even extending to the case where r_{sh} is comparable to r_e.[6] To avoid complications associated with inferring density from the electron saturation portion of the characteristic when operating in a magnetic field using conventional analysis techniques, ion saturation current is often used instead where,

$$I_{ion} = A_p e n_0 \sqrt{\frac{T_e}{m_e}} e^{-0.5} \tag{8}$$

The factor $e^{-0.5} = e^{-e\varphi/Te}$ arises from the density decrease at the sheath edge (where quasineutrality applies at the bulk plasma) to the pre-sheath. With the ion flow velocity at the sheath edge taken as the ion sound speed, ion energy and flux conservation requires approximately that $e\phi(r_{sh}) = T_e/2$ and the Boltzmann condition then allows,

$$n_{ion}(r_{sh}) = n_0 e^{\frac{-e\varphi(r_{sh})}{T_e}} = n_0 e^{-0.5} \tag{9}$$

Since the ion gyroradius is typically much larger than probe dimensions, and if the sheath is small, there is no effect on I_{ion} from a large range of magnetic field magnitudes. The value determined however may still be compromised by the structure of the fitting routine used to analyze the characteristic i.e., density determined from even the ion saturation level can be incorrect since the data reduction technique typically applies a fit to the entire IV characteristic, a portion of which is the electron saturation current region. Also, the existence of a high energy electron component added to the bulk population can complicate this analysis[8] but for a MB distribution the analysis is justified.

IV.3 - Resonance probe determinations of T_e, n_e using f(ε)

In addition to determining n_e with the resonant probe techniques based on electron plasma resonance, we are also able to determine plasma potential, V_p, and T_e based on construction of the electron energy distribution as outlined above and in cited works. In many cases of practical interest we are simply able to use the $Re(Z_{ac})$ output of the network analyzer as seen in Eqs. (2) and (3) when the approximation that $(\omega R_{ac} C_{ac})^2 << 1$ is valid. We stress that C_{ac} seen in Eq. (3) is determined from experimental values with the exception of an assumption of a constant bulk plasma inductance L_p[4]. For comparison purposes we show in each plot of Figure 3 two experimental determinations of $f(\varepsilon)$ using, in one case, R_{ac} , and in the other $Re(Z_{ac})$. These cases correspond in Eq (2) to the situation where the condition above is not rigorously satisfied and in fact is on the order of 1 itself even for the lower frequency ranges. Citing a typical value we allow $C_{ac} \sim 2 \times 10^{-11}$ F, $f = 3$ MHz ($\omega = 2\pi f$) and $R_{ac} \sim 2000\ \Omega$. In this example $(\omega R_{ac} C_{ac})^2 \sim 0.56$ and so we should suspect some difference in the construction of $f(\varepsilon)$ depending on whether we choose $Re(Z_{ac})$ or R_{ac} in Eq. (2). Examination of each of the plots demonstrates that the difference is minimal and only begins show deviation when the applied bias becomes larger. As a result, the effect on the determination of n_e and the average energy is minimal for this parameter range based on the choice of method employed. We note that the construction of $f(\varepsilon)$ depends on the 1rst derivative of R_{ac}^{-1} (or $Re(Z_{ac})^{-1}$) and not on the function itself.

Figure 4 shows a comparison among the three methods of determining n_e from: (1) the Langmuir probe sweep, (2) the resonance peak and, (3) integration of $f(\varepsilon)$. Figure 5 shows comparison of the Langmuir probe sweep to determine T_e versus estimating it as $T_e = 2/3\ E_{av}$ where E_{av} , the average energy, is found buy integration over $\varepsilon f(\varepsilon)$. (Note that the abscissa of Figures 4 and 5 is applied frequency. The reason for this is for consistent representation of measurements taken using the Langmuir probe sweep, *i.e.*, a value for n_e , T_e was determined before each sweep of the bias voltage for a given frequency. Since the other methods determine a single value only, they appear as a straight line on each plot.) Comparing both cases of the resonance peak determination of n_e shows a higher value as would be expected from the Langmuir probe analysis if there is a magnetic field effect on sheath collection due to orientation as discussed above, However, integration of the distribution function yields a value closer to that obtained by the Langmuir probe sweep analysis. The reason for this is not immediately evident. One possible explanation lies in the fact that the construction of $f(\varepsilon)$ is limited insofar as the range of bias voltage covered due to experimental noise limitations at lower frequencies. This suggests we are "missing" a tail of the distribution further suggesting that the integration of $f(\varepsilon)$ yields a value less than is the actual case.

IV.4 $Re(Z_{ac})$ vs V_{bias} at fixed frequencies

Finally, Figure 6 shows $Re(Z_{ac})$ *vs* V_{bias} at fixed frequencies. As described briefly above and in the works cited, this is the primary plot from which plasma potential is obtained and from which the values of $Re(Z_{ac})$ arise for use in the construction of $f(\varepsilon)$. The local minima at approximately 2 volts in this figure are consistent with the determination of V_p from the Langmuir probe-based characteristic.

V. Summary

We have developed an impedance probe technique for determining electron density, temperature, plasma potential and the electron distribution function over the past three years in studies using as rf impedance probes spheres of different sizes. The theoretical basis for this work found in the references in ***Section VII*** suggests that the technique is, to a large degree, independent of probe geometry. The work presented here, using a cylindrical probe with a high-aspect ratio, is consistent with this conclusion.

VI. Figure Captions

Figure 1 – The real part of the complex plasma impedance, $Re(Z_{ac})$, plotted versus the applied network analyzer rf frequency for two separate experimental series. The primary resonance occurs at the bulk plasma electron frequency. Resonances of lower amplitude are produced by the chamber wall reflections and are unrelated to the bulk plasma.

Figure 2 – The imaginary part of the complex plasma impedance. $Im(Z_{ac})$, plotted versus the applied network analyzer rf frequency for two separate experimental series using a 15 cm x 0.16 cm (length x radius) cylinder. The zero crossings occur at the bulk plasma electron frequency. As with the $Re(Z_{ac})$ structures in either the capacitve or inductive reactance are associated with chamber wall reflections and are unrelated to the bulk plasma.

Figure 3 – Plots of the electron distribution function $f(\varepsilon)$ vs applied probe bias for an analyzer sweep frequency of 3 MHz as determined by 2 separate methods: (1) The black curve shows $f(\varepsilon)$ using $Re(Z_{ac})$ in Eq. (2) and, (2) the red curve shows $f(\varepsilon)$ using R_{ac} in Eq. 2. The significance of this is described in the body of the text.

Figure 4 – The bulk electron plasma density, n_e , as determined by 3 separate methods indicated on the figure: (1) The data points are for separate voltage sweeps using the cylinder as a Langmuir probe, (2) The red line is the value of n_e as determined by the resonances shown in Figures 1 and 2 and, (3) The green line is the value of n_e as determined by integration of the distribution function shown in Figure 6. Construction of the distribution function is described in the body of the paper.

Figure 5 – Plots of the electron temperature, T_e , as determined by 2 separate methods indicated on the figure: (1) The data points are T_e as determined by conventional Langmuir probe analysis and, (2) The red line is T_e as determined by integration of the electron distribution function to obtain the average energy. Construction of the distribution function is described in the body of the paper.

Figure 6 – Plots of the $Re(Z_{ac})$ for frequency scans varying from 2 to 9 MHz vs applied bias voltage for two separate experimental series. For both runs the plasma potential determined from Langmuir probe data, $\varphi_p \sim 2$ V, corresponding to the local minimum at this bias in both plots shown.

VII. References

[1]D.N. Walker, R.F. Fernsler, D.D. Blackwell, W.E. Amatucci, and S.J. Messer, *Phys. Plasmas* **13**, 032108 (2006)

[2]D.N. Walker, R.F. Fernsler, D.D. Blackwell, W.E. Amatucci, *Phys. Plasmas* **15**, 123506 (2008)

[3]D.N. Walker, R.F. Fernsler, D.D. Blackwell, W.E. Amatucci, *Phys. Plasmas* **17**, 113503 (2010)

[4]D.N. Walker, R.F. Fernsler, D.D. Blackwell, W.E. Amatucci, *NRL Memorandum Report*, **6750-10-9237** (2010)

[5]J.G. Laframboise, (PhD Thesis) Univ. of Toronto, *Institute for Aerospace Studies, Report No. 100*, (1966)

[6]E.P. Szuszcewicz and P.Z. Takacs, *Phys. of Fluids*, **22**(12), 2424 (1979)

[7]M.J. Druyvesteyn, *Physica* **10**, 69, 1930

[8]R.F. Fernsler, *Plasma Sources Sci. and Technol*, **18**, 014012 (2009)

VIII. Figures

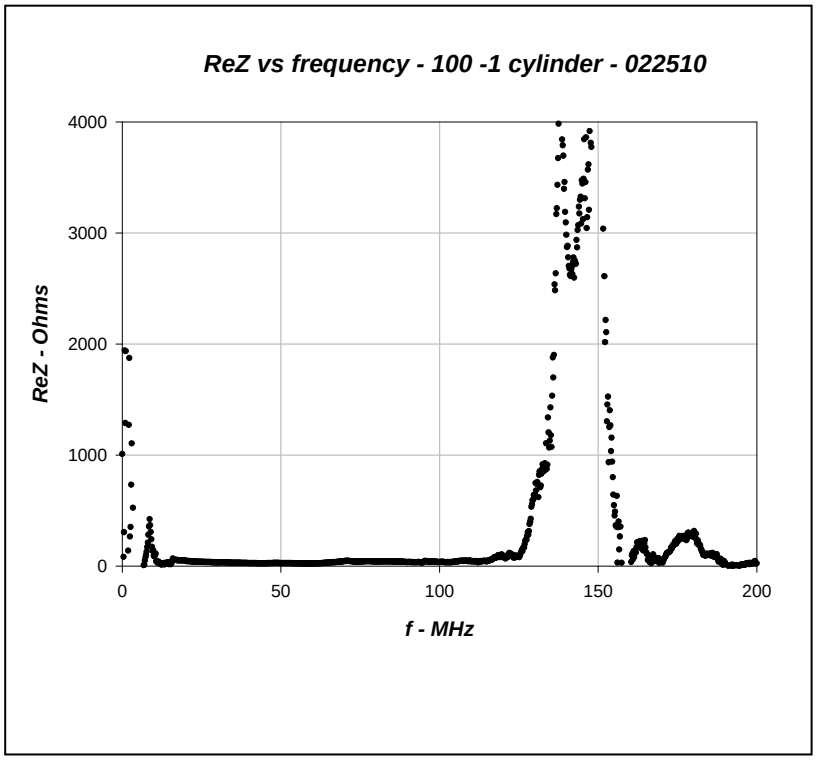

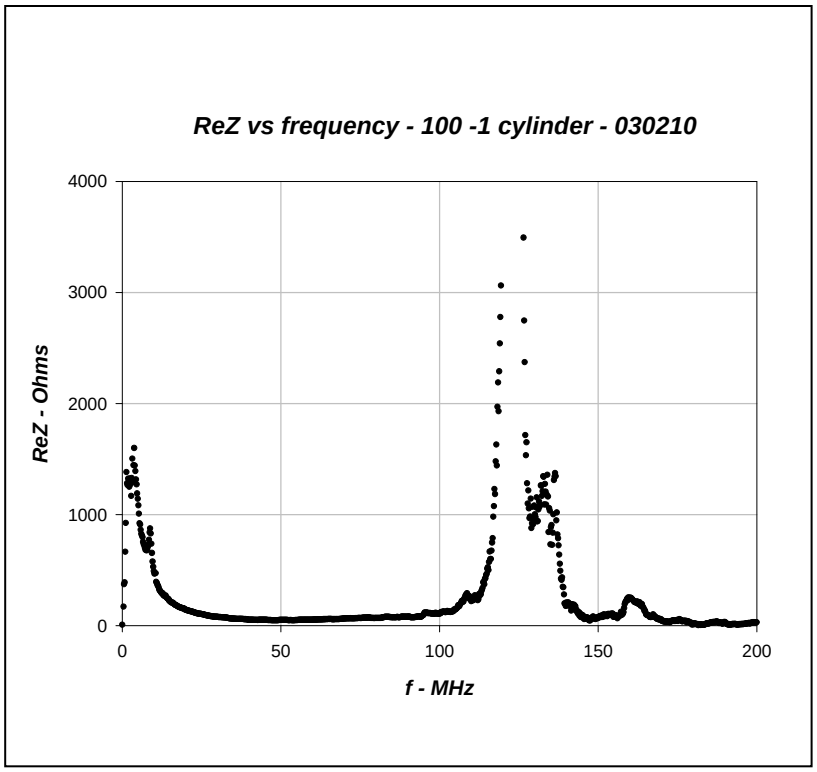

Figure 1

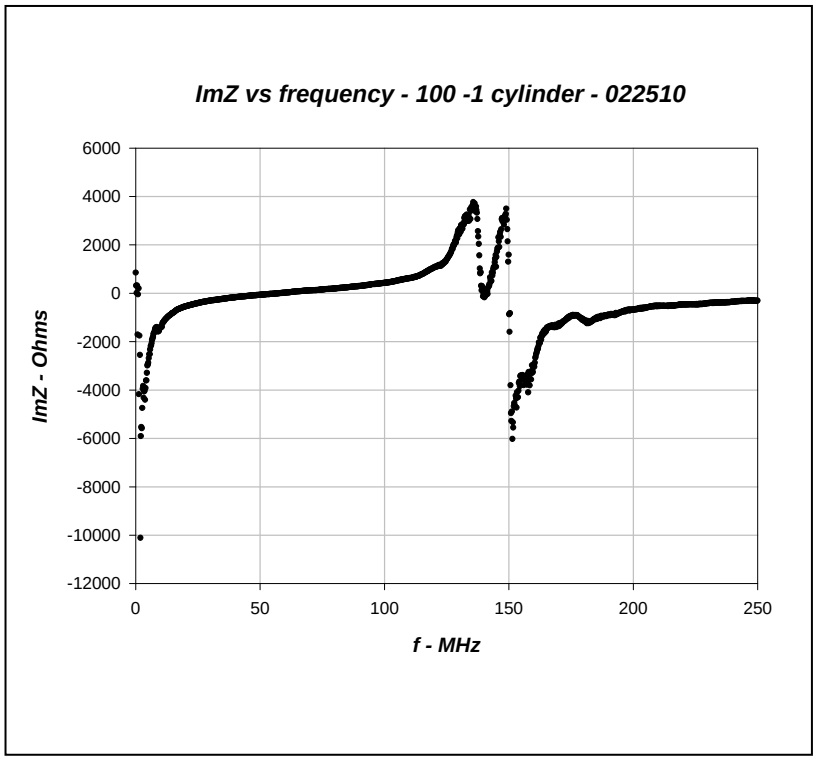
ImZ vs frequency - 100 -1 cylinder - 022510
ImZ - Ohms
6000
4000
2000
0
-2000
-4000
-6000
-8000
-10000
-12000
0
50
100
150
200
250
f - MHz

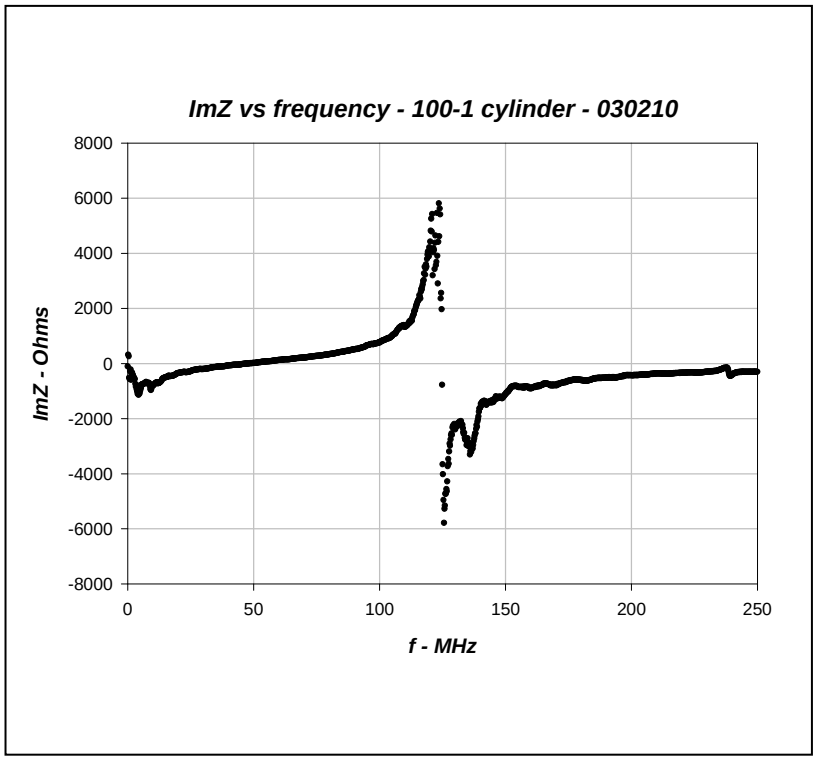
ImZ vs frequency - 100-1 cylinder - 030210
ImZ - Ohms
8000
6000
4000
2000
0
-2000
-4000
-6000
-8000
0
50
100
150
200
250
f - MHz

Figure 2

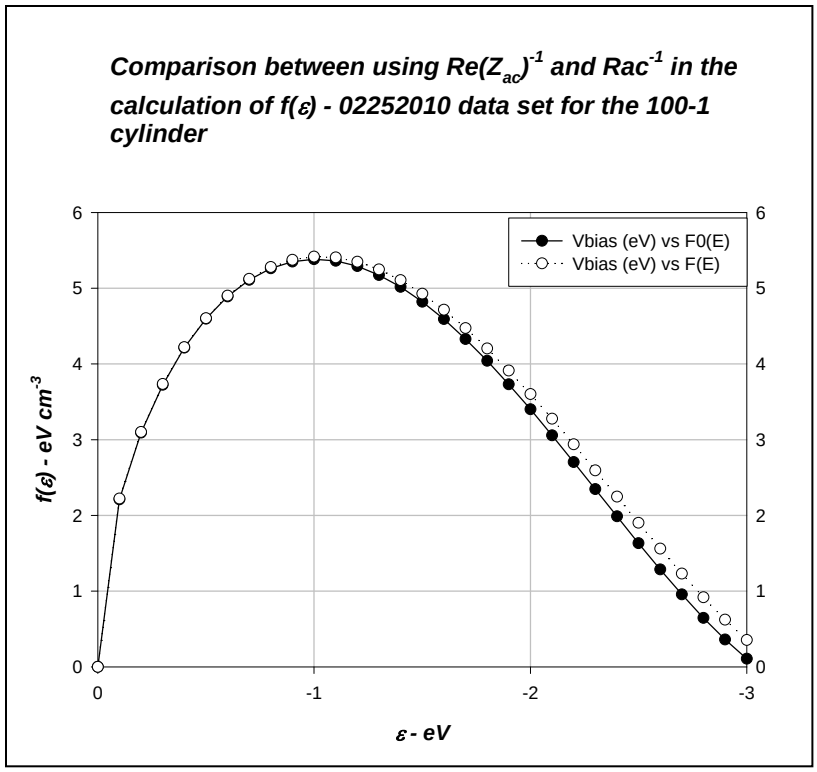
Comparison between using Re(Z_ac)^-1 and Rac^-1 in the calculation of f(ε) - 02252010 data set for the 100-1 cylinder
Vbias (eV) vs F0(E)
Vbias (eV) vs F(E)
f(ε) - eV cm^-3
ε - eV
0
1
2
3
4
5
6
-1
-2
-3

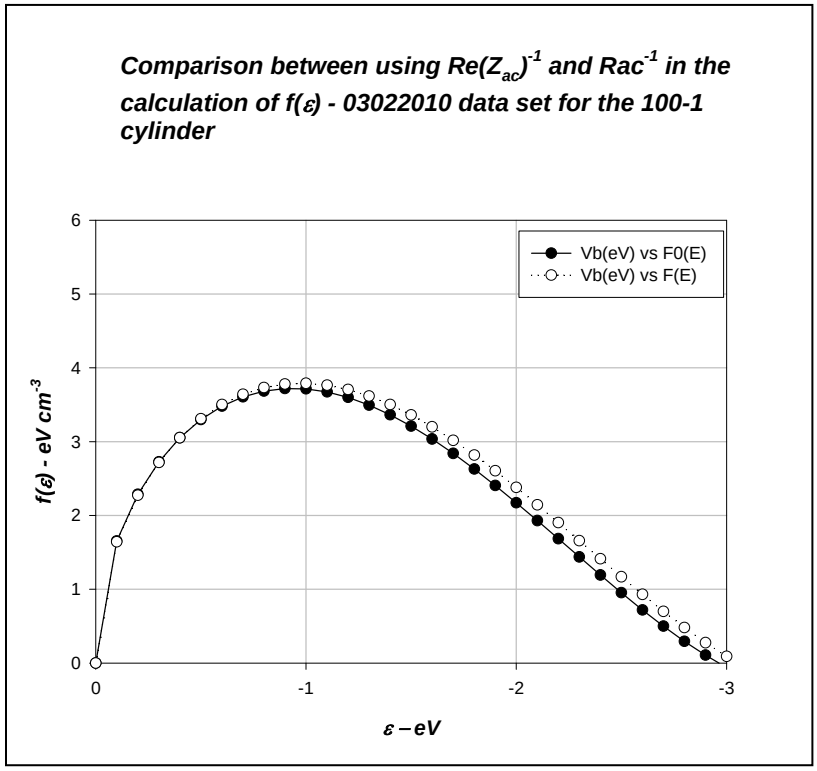
Comparison between using Re(Z_ac)^-1 and Rac^-1 in the calculation of f(ε) - 03022010 data set for the 100-1 cylinder
Vb(eV) vs F0(E)
Vb(eV) vs F(E)
f(ε) - eV cm^-3
ε – eV
0
1
2
3
4
5
6
-1
-2
-3

Figure 3

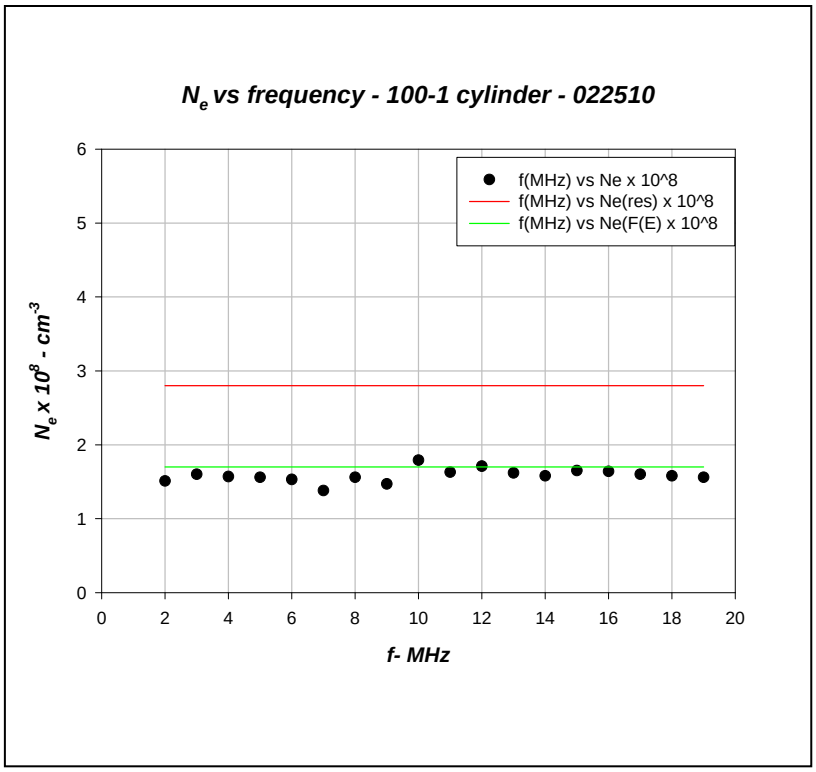
N_e vs frequency - 100-1 cylinder - 022510
f(MHz) vs Ne x 10^8
f(MHz) vs Ne(res) x 10^8
f(MHz) vs Ne(F(E) x 10^8
N_e x 10^8 - cm^{-3}
f- MHz

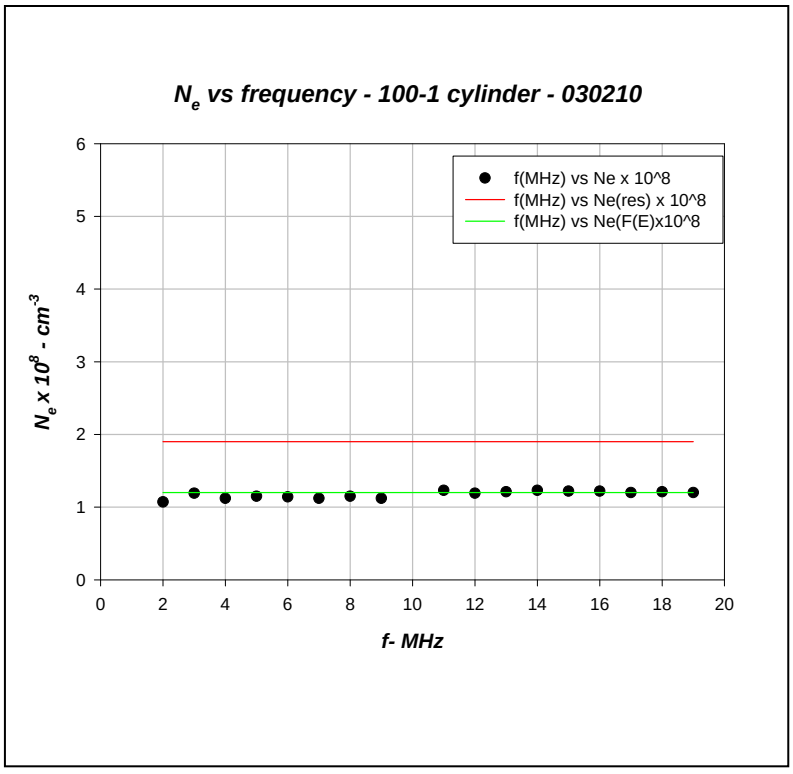
N_e vs frequency - 100-1 cylinder - 030210
f(MHz) vs Ne x 10^8
f(MHz) vs Ne(res) x 10^8
f(MHz) vs Ne(F(E)x10^8
N_e x 10^8 - cm^{-3}
f- MHz

Figure 4

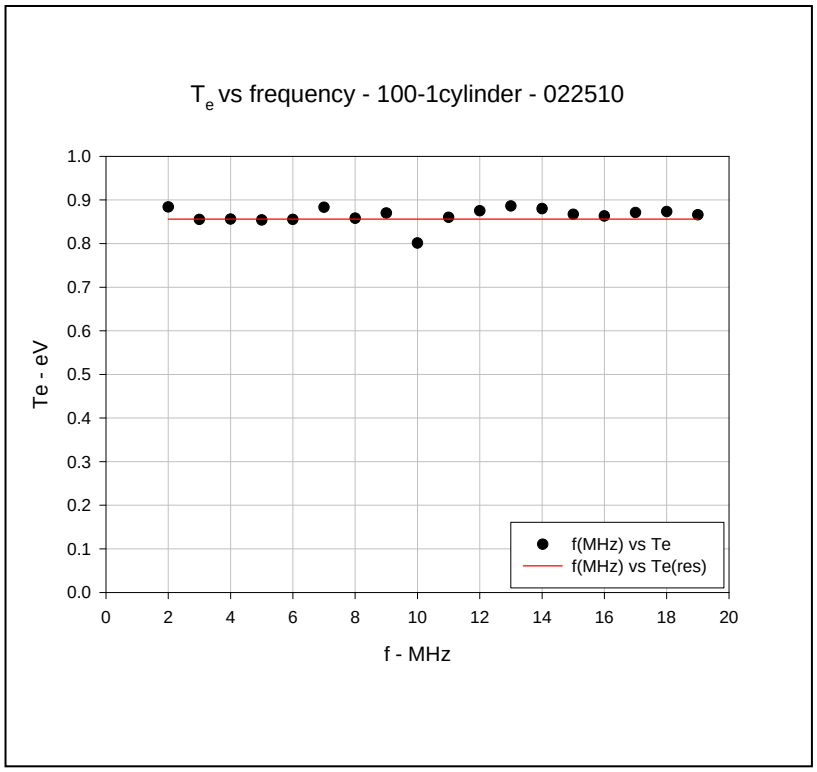
T_e vs frequency - 100-1cylinder - 022510
Te - eV
f - MHz
f(MHz) vs Te
f(MHz) vs Te(res)

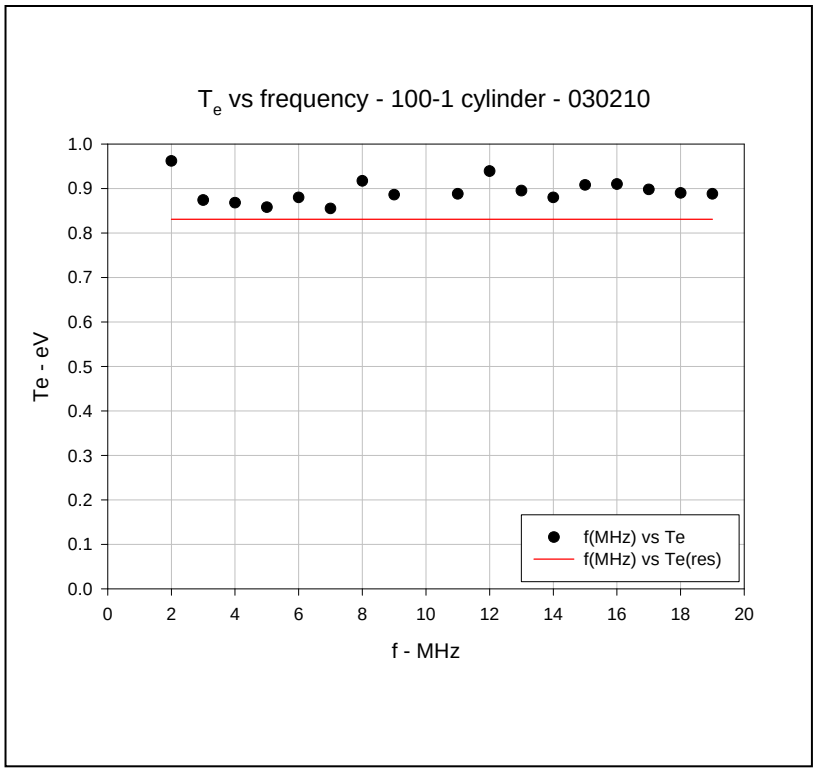
T_e vs frequency - 100-1 cylinder - 030210
Te - eV
f - MHz
f(MHz) vs Te
f(MHz) vs Te(res)

Figure 5

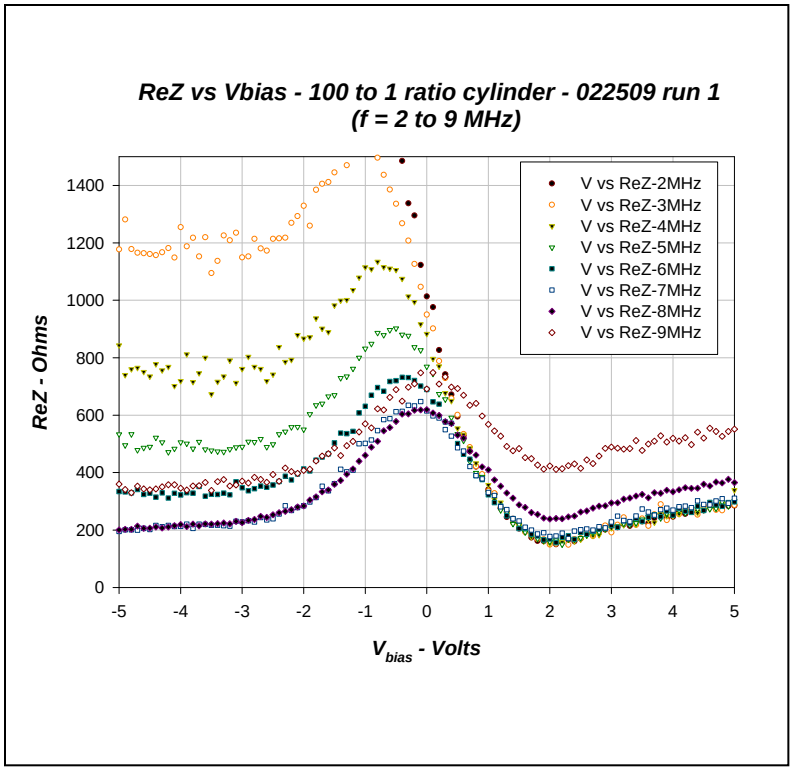
ReZ vs Vbias - 100 to 1 ratio cylinder - 022509 run 1
(f = 2 to 9 MHz)
ReZ - Ohms
V bias - Volts
V vs ReZ-2MHz
V vs ReZ-3MHz
V vs ReZ-4MHz
V vs ReZ-5MHz
V vs ReZ-6MHz
V vs ReZ-7MHz
V vs ReZ-8MHz
V vs ReZ-9MHz

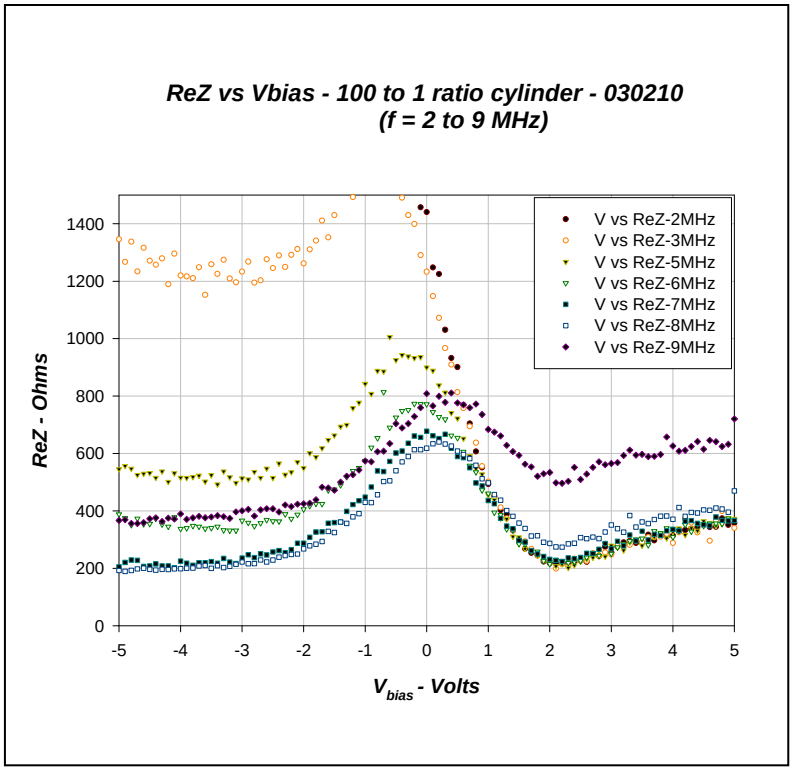
ReZ vs Vbias - 100 to 1 ratio cylinder - 030210
(f = 2 to 9 MHz)
ReZ - Ohms
V bias - Volts
V vs ReZ-2MHz
V vs ReZ-3MHz
V vs ReZ-5MHz
V vs ReZ-6MHz
V vs ReZ-7MHz
V vs ReZ-8MHz
V vs ReZ-9MHz

Figure 6